Electronic Supplementary Material (ESI) for RSC Advances.


# Supplementary Information

## Synthesis of Uniform Rare Earth Doped $Gd_2O_2S$ Sub-micron Sized Spheres Using Gas-Aided Sulfurization and its Optical Characteristics

Shuqing He†, Xinyu Zhao†, and Mei Chee Tan*

Engineering Product Development, Singapore University of Technology and Design,
8 Somapah Road, Singapore 487372.

†Authors contributed equally to this work.

*To whom correspondence should be addressed, meichee.tan@sutd.edu.sg

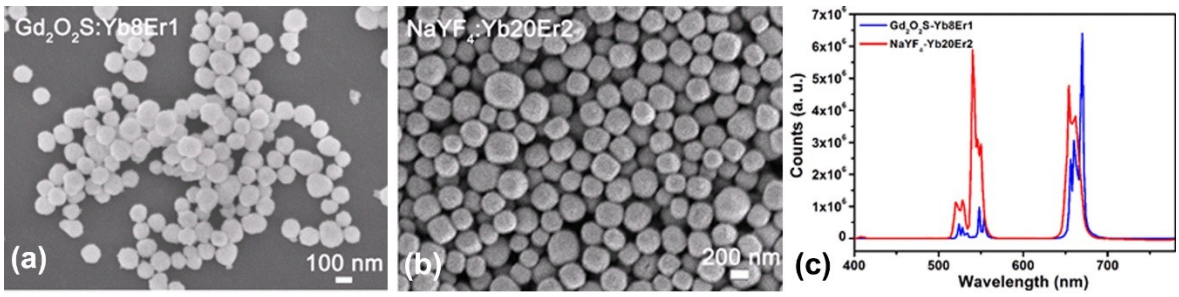


Figure S1. SEM images of (a) $Gd_2O_2S$:Yb8Er1 (~118 nm) and (b) $NaYF_4$:Yb20Er2 (~275 nm) synthesized at our laboratory. The $NaYF_4$ samples with an identical spherical shape was prepared by a hydrothermal method using sodium citrate as a surfactant as reported in one of our earlier works.[1] (c) The upconversion emission steady state spectra of both materials are shown, where the emission fine structure of the visible emissions was also slightly more obvious in the $Gd_2O_2S$ host system. Reference 1: Y. Sheng, L.-D. Liao, N. Thakor and M. C. Tan, Sci. Rep., 2014, 4. 6562.

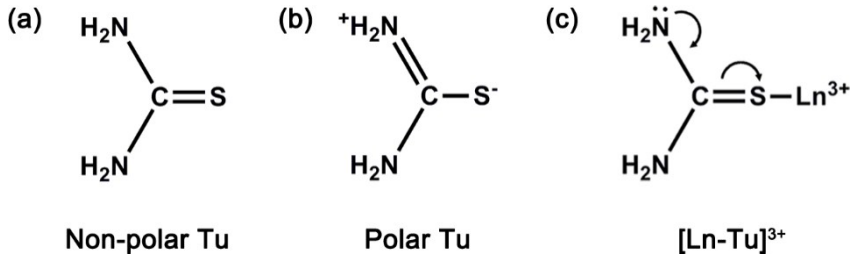


Figure S2. Chemical structure of (a) non-polar thiourea (Tu), (b) polar Tu and (c) lanthanide (Ln)-Tu complex. The formation of S–$Ln^{3+}$ bonds which results in the C=S stretching of Tu shift to lower wavenumbers compared to that of pure Tu.

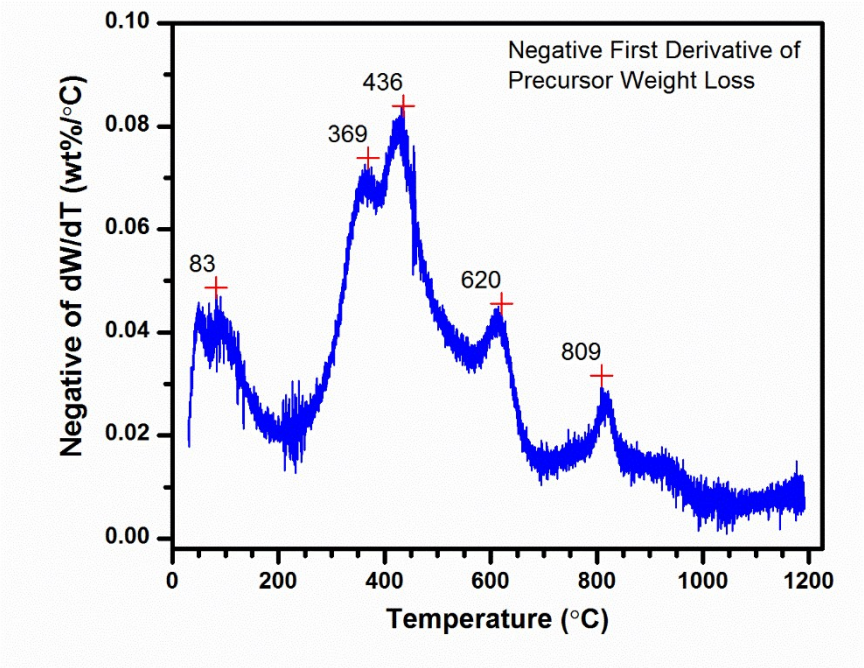


Figure S3. Negative first derivative of TGA curve of precursor shows the points of inflection which mark the regions where major weight loss events were observed.

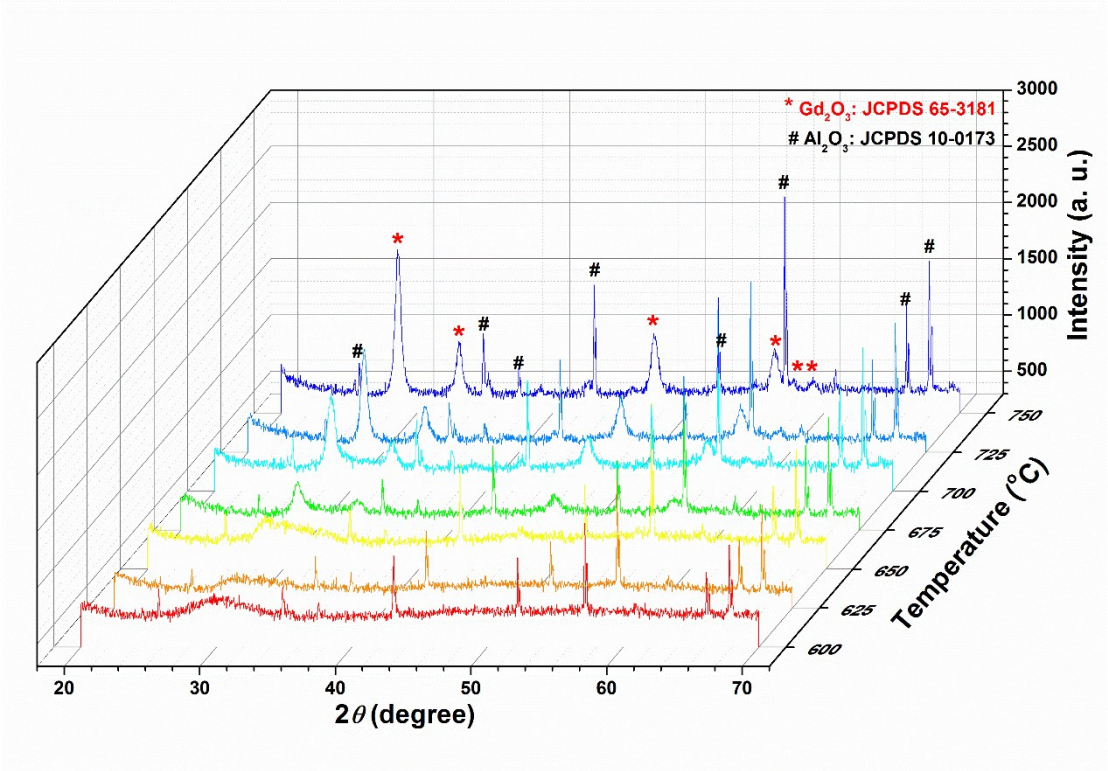


Figure S4. XRD patterns of the precursor that was heated in vacuum at different temperature of 600–750 °C. Reference powder diffraction files of $Gd_2O_3$ from JCPDS 65-3181 and $Al_2O_3$ from JCPDS 10-0173 were used. The results show that the amorphous-to-crystalline phase transition temperature in vacuum was ~675°C

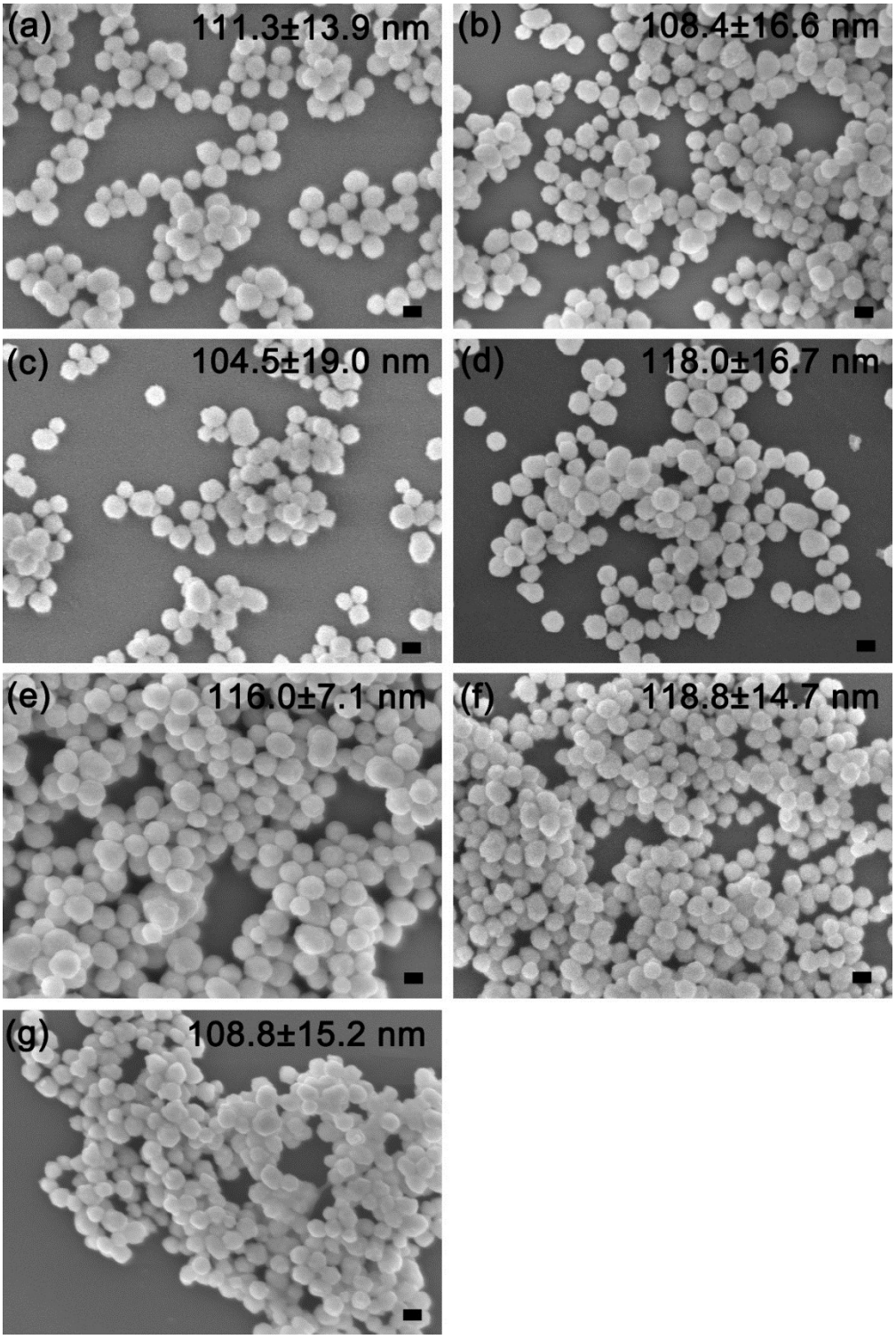


Figure S5. SEM images show that the particles retain the original morphology during the heat treatment process at different temperature, which is due to the PVP coating acting as a sintering inhibitor. SEM images of $Gd_2O_2S$ samples prepared at different temperatures: (a) 500°C, (b) 600°C, (c) 700°C, (d) 800°C, (e) 900°C, (f) 1000°C, and (g) 1100°C. Scale bar represents 100 nm. Some particle shrinkage (from average sizes of 122 to 104-118 nm) was observed, which could be due to the decrease in solid volume during the amorphous-to-crystalline phase transition.

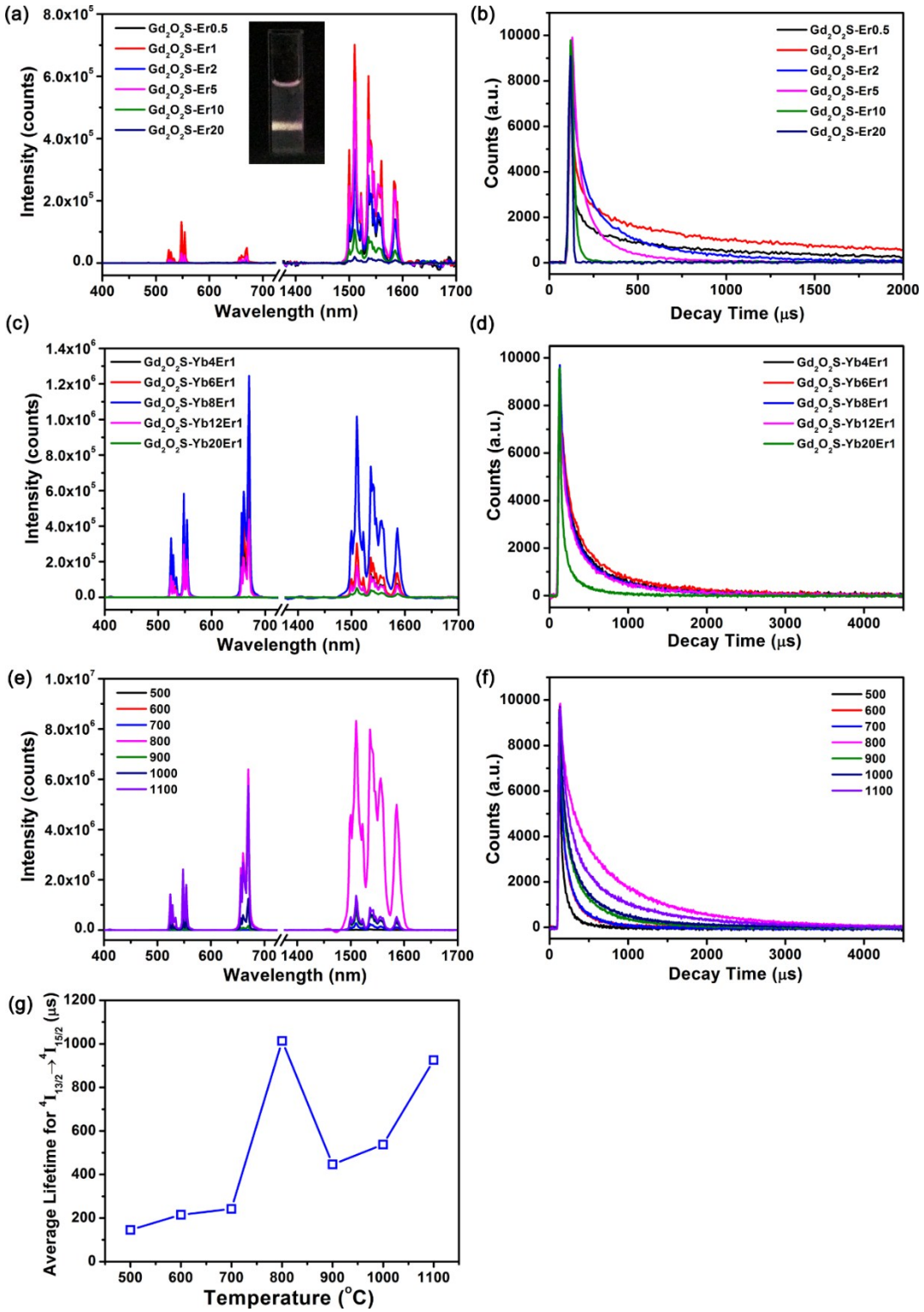


Figure S6. Steady state luminescence (a, c, and e) and time-resolved luminescence spectra (b, d, and f) of (a, b) Er doped $Gd_2O_2S$ and (c, d) Yb,Er co-doped $Gd_2O_2S$ samples prepared at 1000°C and (e, f) $Gd_2O_2S$:Yb8Er1 samples prepared using different heat treatment temperatures. Inset in (a) is Photograph of $Gd_2O_2S$:Yb,Er sample dispersed in dimethyl sulfoxide (~3 mg/mL) illuminated using a 975 nm laser at ~2700 mW. (g) Fitted decay time of $Gd_2O_2S$:Yb8Er1 samples prepared using different heat treatment temperatures.

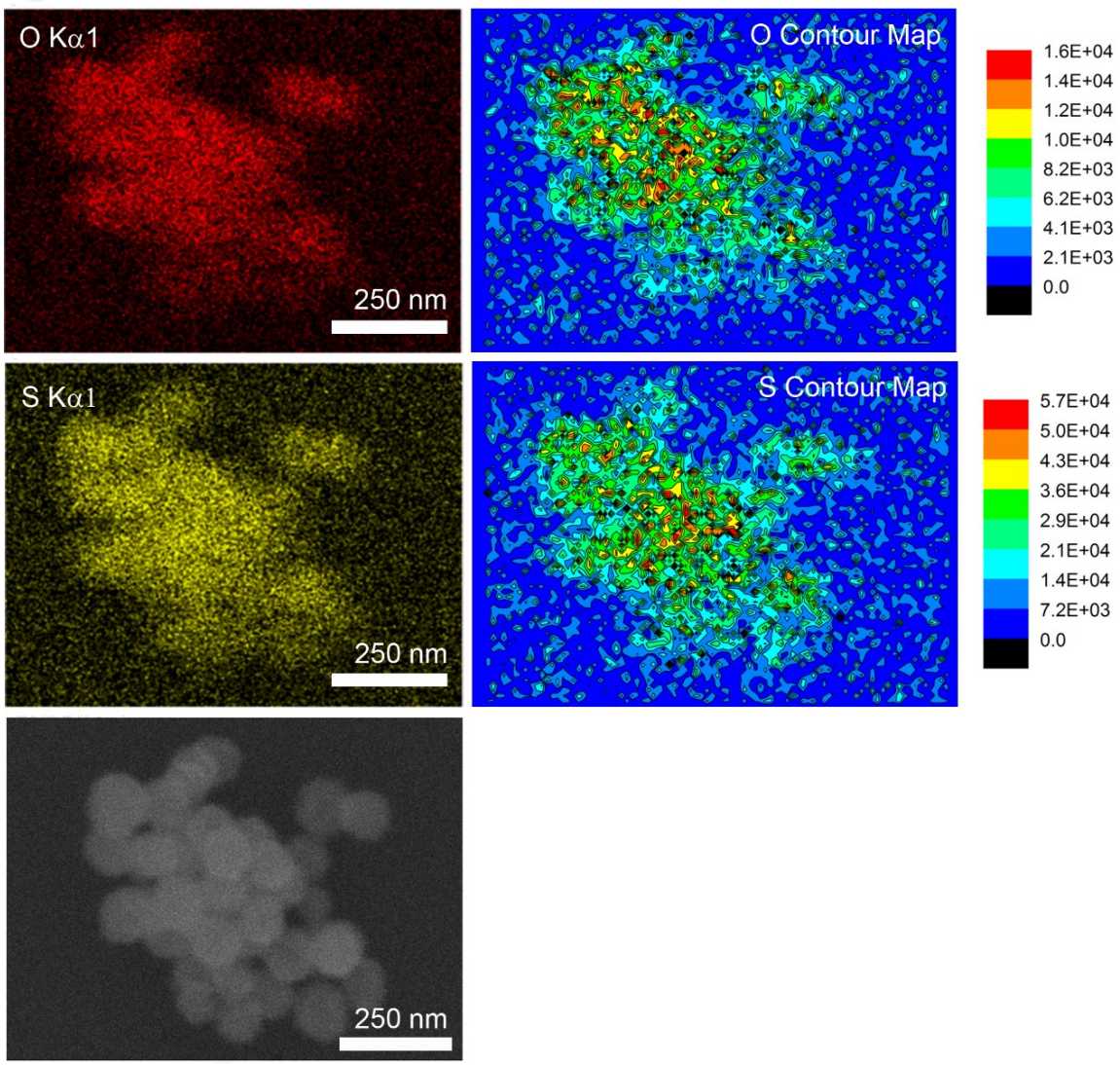


Figure S7. EDX elemental maps and corresponding contour map of $Gd_2O_2S$:Er20 sub-microparticles. The bottom panel shows the corresponding SEM image of the powders where the EDX elemental maps were obtained from.

Table S1. Measured relative composition of Gd and Yb+Er in $Gd_2O_2S$ samples doped with different Yb and Er concentrations calculated from EDX spectrum. Yb6Er1 represents the dopant concentration of Yb = 6 mol% and Er = 1 mol%. The signals and peaks of Yb-Er could not be accurately decoupled and the Yb-Er composition for $Gd_2O_2S$:Yb4Er1 could not be measured as it was below the instrument's measurement limit of 5 mol%. The elemental compositions of O and S are not accurate and are therefore not shown, since it can be found in most common contaminants.

| | **Yb6Er1** | | **Yb8Er1** | | **Yb12Er1** | | **Yb20Er1** | |
|---|---|---|---|---|---|---|---|---|
| | **Designed Relative Ln Ratio (%)** | **Measured Relative Ln Ratio (%)** | **Designed Relative Ln Ratio (%)** | **Measured Relative Ln Ratio (%)** | **Designed Relative Ln Ratio (%)** | **Measured Relative Ln Ratio (%)** | **Designed Relative Ln Ratio (%)** | **Measured Relative Ln Ratio (%)** |
| Gd | 93 | 91.4 | 91 | 88.8 | 87 | 94.4 | 79 | 72.4 |
| Yb+Er | 7 | 8.6 | 9 | 11.2 | 13 | 5.6 | 21 | 27.6 |

Table S2. The lower the number of phonons required to bridge the energy gap, the more likely non-radiative transitions are possible

| **Er Transitions** | **Energy Difference ($cm^{-1}$)** | **Number of Phonons** |
|---|---|---|
| $^4F_{7/2} \rightarrow {}^2H_{11/2}$ | 1380 | 2 – 3 |
| $^2H_{11/2} \rightarrow {}^4S_{3/2}$ | 767 | 1 – 2 |
| $^4S_{3/2} \rightarrow {}^4F_{9/2}$ | 3120 | 6 – 7 |
| $^4I_{11/2} \rightarrow {}^4I_{13/2}$ | 3640 | 7 – 8 |